Article:

Stap, LB, de Boer, B, Ziegler, M et al. (3 more authors) (2016) CO2 over the past 5 million years: Continuous simulation and new δ11 B-based proxy data. Earth and Planetary Science Letters, 439. pp. 1-10. ISSN 0012-821X

https://doi.org/10.1016/j.epsl.2016.01.022

CO_2 over the past 5 million years: continuous simulation and new δ^{11}B-based proxy data

Lennert B. Stap[1,*], Bas de Boer[1,2], Martin Ziegler[3,4], Richard Bintanja[5], Lucas J. Lourens[3], Roderik S. W. van de Wal[1]

Abstract

During the past five million years, benthic δ^{18}O records indicate a large range of climates, from warmer than today during the Pliocene Warm Period to considerably colder during glacials. Antarctic ice cores have revealed Pleistocene glacial-interglacial CO_2 variability of 60-100 ppm, while sea level fluctuations of typically 125 m are documented by proxy data. However, in the pre-ice core period, CO_2 and sea level proxy data are scarce and there is disagreement between different proxies and different records of the same proxy. This hampers comprehensive understanding of the long-term relations between CO_2, sea level and climate. Here, we drive a coupled climate-ice sheet model over the past five million years, inversely forced by a stacked benthic δ^{18}O record. We obtain continuous simulations of benthic δ^{18}O, sea level and

[*]Corresponding author. Tel.: +31 30 253 3167, email: L.B. Stap@uu.nl

[1]Institute for Marine and Atmospheric research Utrecht (IMAU), Utrecht University, Princetonplein 5, 3584 CC Utrecht, The Netherlands

[2]School of Earth and Environment, Faculty of Environment, University of Leeds, LS2 9JT Leeds, United Kingdom

[3]Department of Earth Sciences, Faculty of Geosciences, Utrecht University, Budapestlaan 4, 3584 CD Utrecht, The Netherlands

[4]ETH Zürich, Geological Institute, Sonneggstrasse 5, 8092 Zürich, Switzerland

[5]Royal Netherlands Meteorological Institute (KNMI), Wilhelminalaan 10, 3732 GK De Bilt, The Netherlands

CO_2 that are mutually consistent. Our model shows CO_2 concentrations of 300 to 470 ppm during the Early Pliocene. Furthermore, we simulate strong CO_2 variability during the Pliocene and Early Pleistocene. These features are broadly supported by existing and new δ^{11}B-based proxy CO_2 data, but less by alkenone-based records. The simulated concentrations and variations therein are larger than expected from global mean temperature changes. Our findings thus suggest a smaller Earth System Sensitivity than previously thought. This is explained by a more restricted role of land ice variability in the Pliocene. The largest uncertainty in our simulation arises from the mass balance formulation of East Antarctica, which governs the variability in sea level, but only modestly affects the modeled CO_2 concentrations.

Keywords:
Carbon dioxide, global climate, global ice volume, sea level,
Plio-Pleistocene, proxy data

1. Introduction

The long-term interactions between CO_2, temperature and sea level are a topical issue in climate science. Recently, there have been a number of attempts to quantify these interactions by studying data from paleo archives. For instance, CO_2 data of Antarctic ice cores and sea level reconstructions from Red Sea sedimentary archives show a close linear correlation over the past 516 ka (Foster and Rohling, 2013). However, an analysis of sea level and temperature records spanning the Cenozoic has indicated a non-linear relation between these variables (Gasson et al., 2012). In the pre-ice core period, CO_2 and sea level data remain scarce. Moreover, uncertainties in

CO_2 reconstructions are large and there is inter-proxy as well as intra-proxy disagreement (Masson-Delmotte et al., 2013; Beerling and Royer, 2011). This limits either the scope or the skill of such reconciling studies.

Benthic forameniferal δ^{18}O records currently provide a more continuous and abundant data source on multi-million year timescales (Lisiecki and Raymo, 2005; Zachos et al., 2008). A complicating factor, however, is the interpretation of benthic δ^{18}O, because it comprises both an ice volume and a deep-sea temperature component. To untangle their relative contributions, two different approaches have been applied so far, namely (1) the use of independent deep-sea temperature proxies such as Mg/Ca of foraminiferal tests, and (2) ice-sheet modeling.

In this study, we expand on the model-based approach to deconvolute the δ^{18}O signal into temperature and sea level, including the simulation of CO_2. We introduce an inverse routine to iteratively calculate CO_2 concentrations over the past five million years from benthic δ^{18}O. The CO_2 is used to drive a recently developed coupled ice sheet-climate model (Bintanja, 1997; De Boer et al., 2010; Stap et al., 2014), which contains a scheme to calculate benthic δ^{18}O. In earlier work, this coupled model has been shown to be capable of reproducing glacial-interglacial cycles of ice volume and temperature over the past 800 kyr in forward mode, using CO_2 from ice cores as input (EPICA community members, 2004; Stap et al., 2014). We now force the model inversely by a stacked benthic δ^{18}O record (Lisiecki and Raymo, 2005), which enables us to study ice sheet-climate interactions in a broader range of climates. This new integrated approach improves upon earlier studies using an inverse benthic δ^{18}O routine (Bintanja and Van de Wal, 2008; De Boer et al., 2010, 2014) by including a climate model in the coupled set-up. It therefore facilitates a better representation of the deep-ocean temperature, as well as the simulation of seasonally-varying meridional-temperature profiles, rather than annual mean and globally uniform temperature perturbations with respect to pre-industrial climate. Moreover, in these earlier studies information on CO_2 was lacking. Taking a hybrid model-data approach, Van de Wal et al. (2011) obtained a continuous CO_2 reconstruction from a log-linear fit between modeled temperature and proxy CO_2 data. Here, however, CO_2 is incorporated in the model as a prognostic variable. Therefore, the simulated CO_2 is mutually consistent with eustatic sea level (ice volume equivalent), and with monthly mean atmospheric and oceanic temperatures, as deduced from benthic $\delta^{18}O$. This improves our understanding of the role of CO_2 in climate variability.

We interpret our simulated CO_2 by studying the long-term relation between CO_2 and global surface air temperature in our model, known as Earth System Sensitivity (ESS), which is affected by the interaction between ice sheets and climate. In addition, we test the sensitivity of our CO_2 simulation to the modeled strength of the meridional ocean overturning, as well as to the formulation of the mass balance of East Antarctica and the relation between deep-sea temperature and $\delta^{18}O$. Finally, we compare our simulated CO_2 to existing CO_2 proxy data (Hönisch et al., 2009; Seki et al., 2010; Bartoli et al., 2011; Martínez-Botí et al., 2015a; Pagani et al., 2010; Zhang et al., 2013; Badger et al., 2013), complemented by a new $\delta^{11}B$-based record.

2. Model and methods

2.1. Coupled ice-sheet-climate model and benthic δ^{18}O calculation

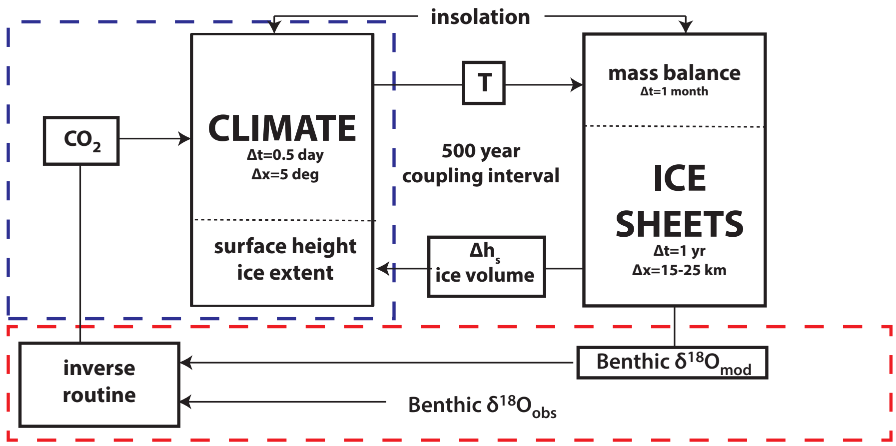

Figure 1: Schematic overview of the coupled model. *Novelties in the set-up with respect to Stap et al. (2014) are marked by a red dashed line, and to De Boer et al. (2010) by a blue dashed line.*

We use a recently developed coupled climate-ice sheet model (Stap et al., 2014). In this coupled set-up, the climate component is represented by a zonally averaged energy balance climate model, developed by Bintanja (1997) based on the model of North (1975). This climate model is tested for sensitivity to some important parameters in Bintanja (1997). It calculates surface temperature in zonal belts of 5° latitudinal and one layer vertical resolution, forced by 1000-yr resolution insolation (Laskar et al., 2004). It uses a radiative transfer scheme and parameterises energy transfer from the equator towards the poles as a diffusive process. Surface albedo is determined by the subdivision of the land surface into (potentially snow covered) grass, forest and land ice. A zonally averaged ocean component of 5° resolution with 6 vertical layers, including a 1.25° thermodynamical sea-ice routine, is used to simulate the large-scale meridional ocean overturning. The ocean overturning strength is variable depending on the temperature difference between the polar and equatorial waters (Stap et al., 2014). The sensitivity of the coupled model to this formulation will be tested in Section 3.2.2.

The climate model is forced by CO_2 yielded by the inverse routine (Section 2.2). As discussed in Stap et al. (2014), the radiative forcing of CO_2 is enhanced by a factor 1.3 to account for the influence of other greenhouse gases (CH_4 and NO_2). The climate model is first run for 500 model years. Thereafter, a one-dimensional ice sheet model is run for the same 500 years. This ice sheet model, described in detail in De Boer et al. (2010), obtains ice velocities from the commonly used Shallow Ice Approximation (SIA). It calculates ice volume and surface height change of the five hypothetical axisymmetrical continents where the major ice sheets grow (North America (NaIS), Eurasia (EuIS), Greenland (GrIS), East-Antarctica (EAIS) and West-Antarctica (WAIS)), including the height-mass-balance feedback. The continents are located at different latitudes and initially they are cone-shaped. Their different centre heights and slopes determine the maximum size and sensitivity to temperature of the ice sheets. The mass balance routine is forced by monthly temperatures (T) from the latitude in the climate model where the ice sheets are located (Stap et al., 2014). Precipitation P is obtained based on the Clausius-Clapeyron equation:

$$P = P_0 e^{0.04T - R/R_c}, \quad (1)$$

where R is the radius of the ice sheet. P_0 and R_c are the present-day precipitation and critical radius respectively. An insolation-temperature melt equation is used to calculate ablation on the different ice sheets:

$$M = [10T + 0.513(1-\alpha)Q + C_{abl}]/100. \quad (2)$$

Here, α is surface albedo, and Q local radiation obtained from Laskar et al. (2004) (Stap et al., 2014). Ice-sheet dependent tuning factors C_{abl} determine the threshold for which ablation starts. In Section 3.3.1 we will test the sensitivity of the model to the C_{abl} value of East Antarctica. All free parameter values (centre height, slope, P_0, R_c and C_{abl}) for the ice sheets are listed in Table 1. In Stap et al. (2014), the tuning targets are discussed.

Table 1: *Model parameters for the ISM: centre height H_{cnt}, slope of the initial bed s, reference precipitation P_0, critical radius R_c, ablation parameter C_{abl}, isotopic sensitivity β_T and isotopic lapse rate β_Z. Starred values indicate parabolic profiles, values given in m^{-1}*

Parameter	Unit	EuIS	NaIS	GrIS	EAIS	WAIS
H_{cnt}	m	1,400	1,400	800	1,450	400
s	-	-0.0000165*	-0.0000115*	-0.0014	-0.0010	-0.0011
P_0	m yr^{-1}	0.88	1.15	1.34	0.71	1.37
R_c	km	1,500	1,800	750	2,000	700
C_{abl}	-	-51	-41	-48	-30	-5
β_T	‰ K^{-1}	0.35	0.35	0.35	0.6	0.8
β_Z	‰ km^{-1}	-6.2	-6.2	-6.2	-11.2	-11.2

After the ice-sheet model has run 500 model years, the climate model receives the ice volume and surface height change (Δh_s) information. This is translated into ice extent, affecting the surface albedo, and surface height at the latitudes where the ice sheets are assumed to be located (Stap et al., 2014). With these new boundary conditions implemented, the climate model runs the next 500 years (Fig. 1). Applying a shorter coupling time interval does not lead to significantly different temperature and sea level output (Stap et al., 2014).

The ice sheet model includes a parameterisation of benthic δ^{18}O values (De Boer et al., 2010) using the following equation:

$$\delta^{18}O = [\delta^{18}O_b]_{PD} - \frac{\overline{\delta^{18}O_i}V_i}{V_o} + \left[\frac{\overline{\delta^{18}O_i}V_i}{V_o}\right]_{PD} + \gamma\Delta T_o. \tag{3}$$

The first term on the right hand side is the observed present-day value of benthic δ^{18}O. The influence of the ice sheets on the signal is represented by the second and third term. Here, V_o and V_i are volume of the ocean and land ice respectively. The following formulation of the isotopic content of the ice sheets is adopted (Cuffey, 2000):

$$\delta^{18}O_i = \delta^{18}O_{PD} + \beta_T\Delta T + \beta_Z\Delta Z. \tag{4}$$

Here, β_T and β_Z are ice-sheet dependent parameters, that determine the influence of annual mean temperature change (ΔT) and surface height change (ΔZ); their values are the same as used by De Boer et al. (2010) (Table 1). Present-day isotopic contents match the modeled values of an earlier study by Lhomme et al. (2005). The final term on the right hand side of Eq. 2 quantifies the influence of deep-sea temperature change with respect to present day (ΔT_o). Gain factor γ is set to 0.28 ‰K^{-1}, taken from a paleotemperature equation (Duplessy et al., 2002). We assess the sensitivity of the model to this value in Section 3.3.3. The deep-sea temperature perturbation is determined from the climate model as the 40-80° N mean of the second vertical ocean layer, representative of the mid-latitude North Atlantic deep ocean.

The energy balance and 1-D ice-sheet models used in our study are less comprehensive than current intermediate complexity (EMICs) and general circulation models (GCMs), and 3-D ice sheet models. However, they have the advantage of allowing for several five-million-year integrations of the coupled ice sheet-climate system, while capturing the relevant large-scale physical processes, notably the interaction between ice sheets and climate (Stap et al., 2014).

2.2. Inverse benthic δ^{18}O routine to calculate CO_2 concentration

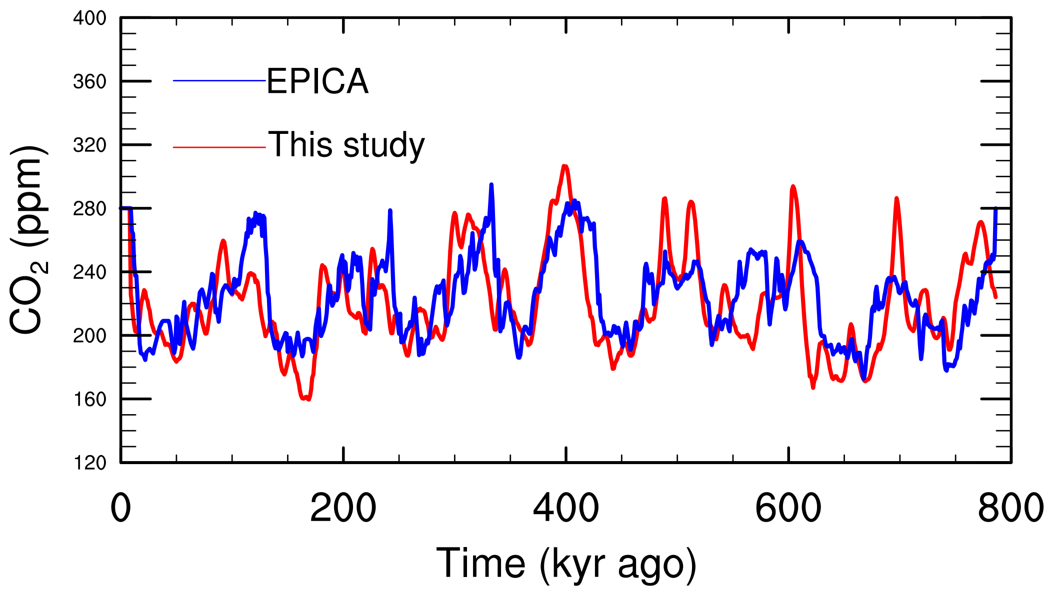

Figure 2: Data-model comparison of CO_2 over the past 800 kyr. *Modeled CO_2 over the past 800 kyr (red), compared to the EPICA ice-core record (EPICA community members, 2004) interpolated to 1000-yr temporal resolution (blue).*

We use an inverse forward modeling approach to calculate CO_2 from benthic $\delta^{18}O$ data. This is achieved by a two-step iterative routine. Each 1000-year cycle starts with an update of the insolation input. At this first iteration step, a new CO_2 concentration is obtained from the difference between the modeled benthic $\delta^{18}O$ value and the observed value 500 years later:

$$CO_2 = \overline{CO_2} * \exp[c * \{\delta^{18}O(t) - \delta^{18}O_{obs}(t + 0.5kyr)\}]. \tag{5}$$

The coupled model is run for 500 model years. Thereafter, as a second iteration step Eq. 5 is applied again. The model is then run for another 500 years, using the updated CO_2, but still forced by the same insolation. While in principle this yields 500 year-resolution CO_2, only the results after the second iteration step are recorded and displayed in this paper. The temporal resolution of the simulated CO_2 is therefore 1000 years. This is the desired resolution, as the physics in our model are not detailed enough to capture sub-millennial climate variations (Stap et al., 2014). We justify excluding the intermediate CO_2 values, by running the model again in forward mode, forced by the 1000-yr resolution simulated CO_2 record; this does not significantly alter the resulting climate and ice volume records.

In Eq. 5, $\overline{CO_2}$ is the mean CO_2 concentration of the preceding 15 kyr, which reflects the long-term timescale of the carbon cycle. Together with parameter c, which is set to $0.45‰^{-1}$, it determines the strength of the response of CO_2 to changes in $\delta^{18}O$. While c is kept constant, it is important to stress that a variable relation between $\delta^{18}O$ and CO_2 is ensured by the carbon-cycle timescale, and most importantly by the second iteration step in the inverse routine. Both the carbon-cycle timescale and c are used to tune the modeled CO_2 over the past 800 kyr to match the EPICA ice-core record (EPICA community members, 2004) (Fig. 2). When 20-kyr running averages of both the simulation and this data are considered, the agreement is very good (Root mean square error (RMSE)=18 ppm, coefficient of determination r^2=0.73). However, also on the original 1000-yr resolution, model and data show reasonable agreement (RMSE=26 ppm, r^2=0.59); the model bias is then -3.9 ppm. For the observed δ^{18}O, we use the stacked record of Lisiecki and Raymo (2005)[LR04], linearly interpolated with a 5-kyr running average to 100-year resolution and smoothed over six data points. The value chosen for c results in the best fit of our modeled δ^{18}O to LR04, with a RMSE of 0.16 (r^2=0.95). Also when only considering the Pliocene (5 to 2.6 Myr ago), a different value for c does not lead to a better agreement with LR04.

2.3. Boron isotope data

Most atmospheric CO_2 proxies suffer from large uncertainties, but the foraminiferal boron isotope based estimates are promising, since they show a good agreement with ice-core data during the Pleistocene (Hönisch et al., 2009). The δ^{11}B of surface dwelling planktic foraminifera is a function of seawater pH, which is in turn related to the CO_2 concentration in the mixed layer. We provide some new Plio-Pleistocene foraminiferal (*G.sacculifer*) δ^{11}B data (Extended Data Table). Our new dataset has a relatively low temporal resolution (on average 250 kyr), but covers a long period from 6.35 until 0.54 Myrs ago and thereby a wide range of CO_2 from 152^{+10}_{-9} to 507^{+46}_{-41} ppm.

2.3.1. Sample locations

Ocean Drilling Program (ODP) Site 1264 (28.53°S; 2.85°E, 2505 m water depth) is located on the central Walvis Ridge in the eastern sector of the South Atlantic subtropical Gyre. ODP Site 1264 is part of a depth transect along the shallow sloping northern flank of Walvis Ridge (Shipboard Scientific Party, 2004), which forms a prominent topographic feature within the Southeast Atlantic Ocean, separating the Angola Basin to the north and the Cape Basin to the south. Preservation of planktic foraminifera in the Plio-Pleistocene sections of Site 1264 is generally good. The age model (Bell et al., 2014) is based on tuning the benthic oxygen isotope record to the LR04 stack (Lisiecki and Raymo, 2005) (Suppl. Data Fig. 1). Today, the surface ocean CO_2 is in equilibrium with the atmosphere.

2.3.2. Analytical methodology

Roughly 50-90 *G.sacculifer* tests (∼20 mg per individual sample) were hand-picked from the 250-355 mm size fraction. In contrast to previous studies (Hönisch et al., 2009; Bartoli et al., 2011), a smaller size fraction had to be used since the sediments generally lacked sufficient numbers of large *G. sacculifers*. It has been suggested that smaller specimen of *G. sacculifer* are susceptible to carbonate dissolution. However, the picked average size, normalized with the weight of the shells of the samples shows no large changes over the record, indicating that dissolution is not biasing the record (Suppl. Data Fig. 2). The tests were crushed between glass plates and cleaned following the protocol of Barker et al. (2003). Cleaned samples were subsequently dissolved in 2N HCL to yield sample solutions with approximately 1 ng of B/ml. Five to eight aliquots of 1 ml solution with 1 ml of boron-free seawater were loaded onto rhenium filaments. Analysis was performed on a Thermal Ionization Mass Spectrometer (Thermo Scientific TRITON) at Lamont Doherty Earth Observatory. Ionization temperature was between 980 and 1020 °C. Samples that showed isotopic fraction exceeding 1‰ over the acquisition time (∼30 minutes) were excluded. The data are standardized against the SRM NIST 951 boric acid standard. All reported δ^{11}B values are based on at least three measurements. Standard errors reported are two internal errors of an in-house consistency standard or two internal errors of repeat analyses of individual sample solutions, if that was larger than the external reproducibility. Two standard errors (2 s.e.) range between 0.28 and 0.7‰ and average 0.33‰ (Extended Data Table).

2.3.3. Determination of pH from δ^{11}B of G.sacculifer

Boron isotope ratios in planktic foraminifera tests are a function of seawater pH. The relative abundance and isotopic composition of the two main dissolved boron species in seawater (borate and boric acid) changes with pH. Since marine carbonates preferentially incorporate the species borate, the boron isotope composition of the carbonate also changes with seawater pH. With a second parameter of the carbonate system (e.g. total alkalinity or carbonate ion concentration), atmospheric pCO_2^{atm} can be inferred from the pH values.

Ocean pH can be calculated from the δ^{11}B of the borate as follows:

$$pH = pK_B - log\left[-(\delta^{11}B_{sw} - \delta^{11}B_{Borate})/(\delta^{11}B_{sw} - \delta^{11}B_{Borate}(^{11,10}K_B - 1)\right], \quad (6)$$

where pK_B is the equilibrium constant for the boric acid/borate system for a given temperature and salinity, $\delta^{11}B_{sw}$ is the isotopic composition of seawater (39.61‰; Foster et al. (2010)), $\delta^{11}B_{Borate}$ is the isotopic composition of the borate ion and K_B is the isotopic fractionation between the two aqueous species of boron in seawater (1.0272±0.0006) (Klochko et al., 2006).

G. ruber Mg/Ca based SSTs for Site 1264 show no apparent trend over the past 5 Myr (Dekens et al., 2012). The reconstructed SSTs for the area in our climate model show a slight cooling trend over the Plio-Pleistocene (around 0.3°C cooling per 1 Myr). We apply these temperatures estimates and a constant salinity of 36 psu in our calculations. We note that these variables have a minor affect on the calculated pH and pCO_2 (∼30ppm for a ±3°C change; ±∼10ppm for a ±3‰ salinity change).

We account for small long-term changes in the boron isotopic composition of seawater ($\delta^{11}B_{sw}$) by using a linear extrapolation between modern $\delta^{11}B$ (39.61‰, Foster et al. (2010)) and the $\delta^{11}B_{sw}$ determined by Foster et al. (2010) for the middle Miocene (12.72 Myr ago, $\delta^{11}B_{sw}$ = 37.8‰). This approach is consistent with Martínez-Botí et al. (2015a).

In order to calculate pH using the equation above, the $\delta^{11}B$ value of the foraminifera has to be corrected for size fraction effect (-2.25‰, Hönisch and Hemming (2004)), and further corrected for a species-specific difference between the $\delta^{11}B_{Borate}$ in ambient seawater and the $\delta^{11}B_{Calcite}$ of the foraminiferal tests. We use an empirical equation for *G.sacculifer* of Martínez-Botí et al. (2015b):

$$\delta^{11}B_{Borate} = (\delta^{11}B_{Calcite} - 3.6)/0.834. \quad (7)$$

The empirical calibration of Martínez-Botí et al. (2015b) is based on δ^{11}B datasets, combining results from MC-ICP-MS with N-TIMS data that were corrected for an analytical offset of 3.32‰. This offset between the two techniques can however not generally be applied. It has been demonstrated that the instrumental offset is matrix dependent (Foster et al., 2013) and can even vary for different foraminifera species (Hönisch et al., 2009). Here, we apply a correction offset of 0.9‰, which is the average offset for foraminifera samples between measurements on the LDEO N-TIMS and the BIG MC-ICP-MS (Foster et al., 2013). The uncertainty in instrument specific offsets and the impact of matrix effects are certainly a major issue in the boron isotope analysis of marine carbonates that needs further investigation. However, it has also been demonstrated that relative differences in δ^{11}B in a sample set of a given matrix can be reconstructed regardless of the applied measurement technique (Foster et al., 2013). Using the corrections above we derive reasonable pH estimates from the Site 1264 samples for the well-constrained Pleistocene part. The uncertainty in pH is dominated by the uncertainty in the δ^{11}B measurement and is on the order of ± 0.04 pH units.

2.3.4. Determination of pCO_2^{atm} *from* δ^{11}B*-derived pH*

To estimate atmospheric pCO_2, a second parameter of the carbonate system is needed. Seki et al. (2010) have compared two different approaches. They reconstructed pCO_2 from modeled $[CO_3^{2-}]$ (Tyrrell and Zeebe, 2004) as well as assuming constant total alkalinity varying with only up to $\pm 5\%$. The comparison between these approaches demonstrates that estimated pCO_2 is relatively insensitive to the second carbonate system parameter and is largely dependent on the recorded pH change as determined by δ^{11}B values. For our calculation we assume a constant total alkalinity of 2300 mmol/kg sea water. The uncertainty in the pCO_2 estimates in largely dominated by the analytical uncertainty in $\delta^{11}B$. Taking into account additional uncertainties in estimated salinity, sea surface temperature and carbonate ion concentration we estimate the uncertainty in the reconstructed pCO_2 on the order of ± 70 ppm in line with earlier studies (Bartoli et al., 2011).

3. Results and Discussion

3.1. Five-million-year simulation

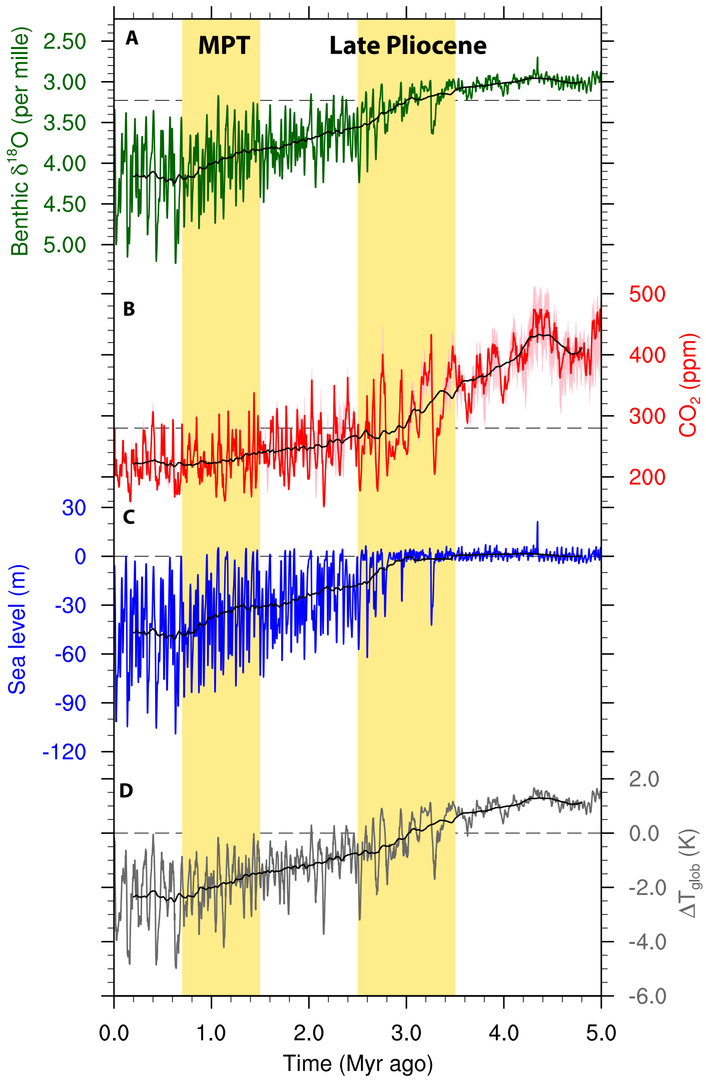

Figure 3: Five-million-year time series of benthic δ^{18}O, CO_2, sea level and global temperature. ***(a)*** *Simulated benthic δ^{18}O (green),* ***(b)***

simulated CO_2 *(red), with error margins based on simulations with increased Antarctic ablation (ABL) and fixed pre-industrial ocean overturning strength (OT) described in Sect. 3.2,* ***(c)*** *simulated sea level in meters above present day (blue),* ***(d)*** *simulated global mean temperature anomaly with respect to PI (T_{glob}; grey). Black lines represent 400-kyr running averages. Highlighted in yellow are the Late Pliocene period 3.5 to 2.5 Myr ago and the Mid-Pleistocene Transition (MPT; 1.5 to 0.7 Myr ago) discussed in the main text.*

Our simulated global mean temperatures during glacials are typically 4 to 5 K below the pre-industrial average (PI), which is consistent with a data reconstruction of the Last Glacial Maximum (Annan and Hargreaves, 2013). In addition, modeled sea-level variability over the past five glacial cycles of 80 to 125 m is in broad agreement with data records (e.g. Grant et al., 2014; Austermann et al., 2013). The modeled CO_2, sea level and global mean temperature records all show decreasing long-term trends over the past 5 Myr, while benthic $\delta^{18}O$ values gradually increase (Fig. 3). During the early Pliocene (5 to 3.3 Myr ago), global mean temperature is up to 1.7 K higher than PI, slightly lower than the 1.8 to 3.6 K range calculated by the PlioMIP GCM ensemble (Haywood et al., 2013).

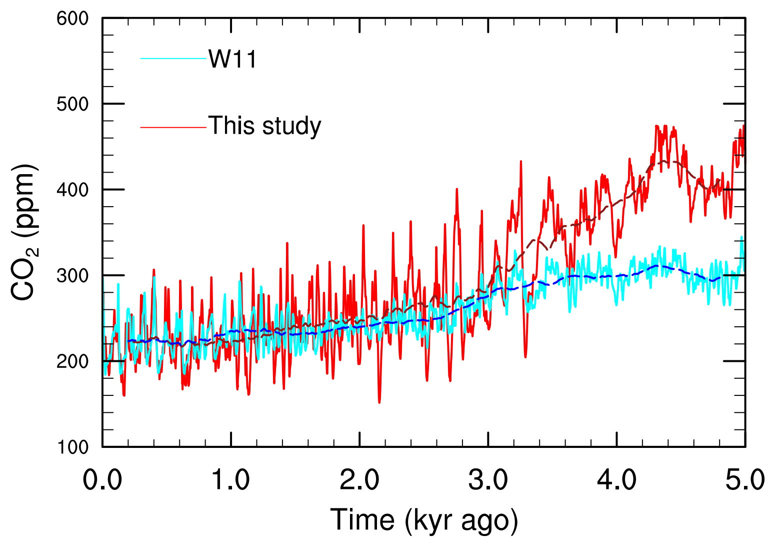

Figure 4: Simulated CO_2 concentrations. *The red line shows our simulated CO_2 record over the past five million years. To compare, the hybrid model-data reconstruction of Van de Wal et al. (2011) is shown (cyan line). Dashed lines represent 400-kyr running averages.*

Our simulation shows CO_2 concentrations of 300 up to 470 ppm during this period (Fig. 4, red line). These levels are considerably higher than found in an earlier reconstruction by Van de Wal et al. (2011) (Fig. 4, [W11] cyan line). In addition, our Pliocene CO_2 exhibits much larger shorter-term variability than this hybrid model-data reconstruction. From the beginning of the Pleistocene (2.5 Myr ago) onwards, the long-term averages of both records nearly coincide. They show a similarly weakly declining trend over the Mid-Pleistocene Transition (1.5 to 0.7 Myr ago), when power in the δ^{18}O spectrum shifts from 41 kyr to 100 kyr (Lisiecki and Raymo, 2005; Zachos et al., 2008; Bintanja and Van de Wal, 2008). Conversely, the higher variability in our simulation continues longer, lasting until the end of the Mid-Pleistocene Transition (0.8 Myr ago). Most prominently, our simulation shows more fiercely falling CO_2 levels during the M2 $\delta^{18}O$ excursion 3.3 Myr ago (415 to 200 ppm) and during the onset of periodic northern hemispheric glaciation 2.7 Myr ago (400 to 180 ppm).

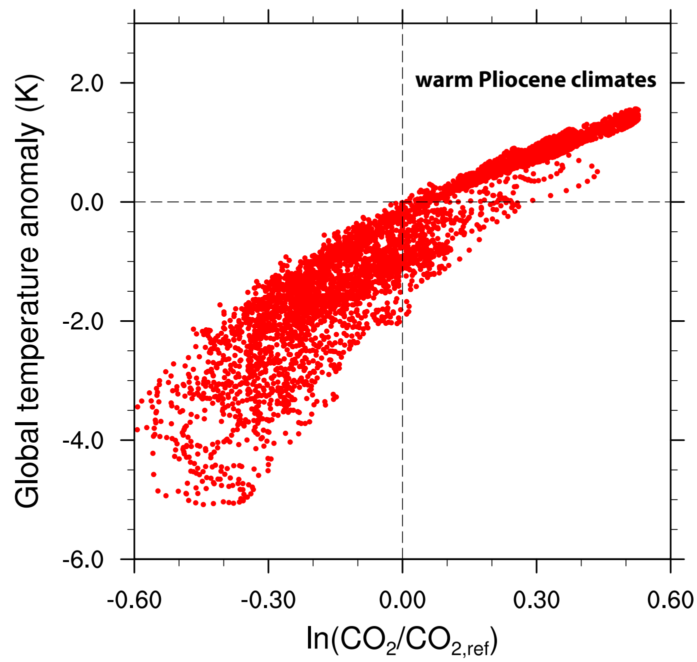

Figure 5: Relation between global temperature anomalies and CO_2. *The relation between logarithmic CO_2 and global temperature perturbations with respect to their pre-industrial (PI) values (280 ppm and 287.7 K respectively) is clearly non-linear in our model.*

The reconstruction by Van de Wal et al. (2011) used the northern hemispheric temperature record of De Boer et al. (2010), which was obtained using an inverse routine forcing the ice sheet model in stand-alone form without climate model. They inferred a constant log-linear relation between this record and several CO_2 proxy data records. We now include a climate model in the set-up and derive CO_2 as a prognostic variable (Fig. 1, dashed blue line). Therefore, Earth System Sensitivity (ESS) is not a priori fixed in our model (Fig. 5). Instead, it is primarily influenced by ice sheet-climate interactions, which we capture in our coupled set-up. During the Pliocene, our simulated CO_2 levels are very variable and show a clear decreasing trend over time (Fig. 3). Meanwhile, ice-volume equivalent sea level is far less variable; its long-term average remains virtually constant, slightly above its present-day value. During this time, in our model the climate is not cold enough for large scale glaciation of the Northern Hemisphere. At the same time, the Antarctic ice sheet has already reached its carrying capacity, the ice sheet size that the continent can maximally sustain (De Boer et al., 2010; Foster and Rohling, 2013). The CO_2 concentrations thus vary between the thresholds for initiation of northern and southern hemispheric glaciation. Through the albedo-temperature feedback, ice volume variability amplifies temperature perturbations, particularly in polar regions (Stap et al., 2014; Masson-Delmotte et al., 2013). Therefore, a reduction of ice volume variability during the Pliocene requires larger changes in CO_2 levels to obtain the same temperature fluctuations (Fig. 5). This implies that ESS is lower during the Pliocene than during the Pleistocene and Holocene in our model, whereas the constant relation between CO_2 and temperature in the record of Van de Wal et al. (2011) connotes the same ESS during these periods. The reduced ESS leads to higher simulated Pliocene CO_2 levels and larger CO_2

variability compared to Van de Wal et al. (2011), as well as compared to Hansen et al. (2013) who used a conceptual δ^{18}O-based climate model and did not take ice-sheet physics explicitly into account. A similar result as ours was obtained by Lunt et al. (2010), who found a reduction of ESS in warmer-than-PI climates (400 ppm CO_2) compared to colder-than-PI climates.

We note that in our model the radiative forcing of CO_2 is enhanced by a factor 1.3 to account for non-CO_2 greenhouse gasses (GHGs). This factor gives accurate results for the ice-core period (Stap et al., 2014), but an increase or decrease in the relative contribution of non-CO_2 is indeterminable in our model. Such a shift would need a compensating opposite change in CO_2.

3.2. Sensitivity analysis

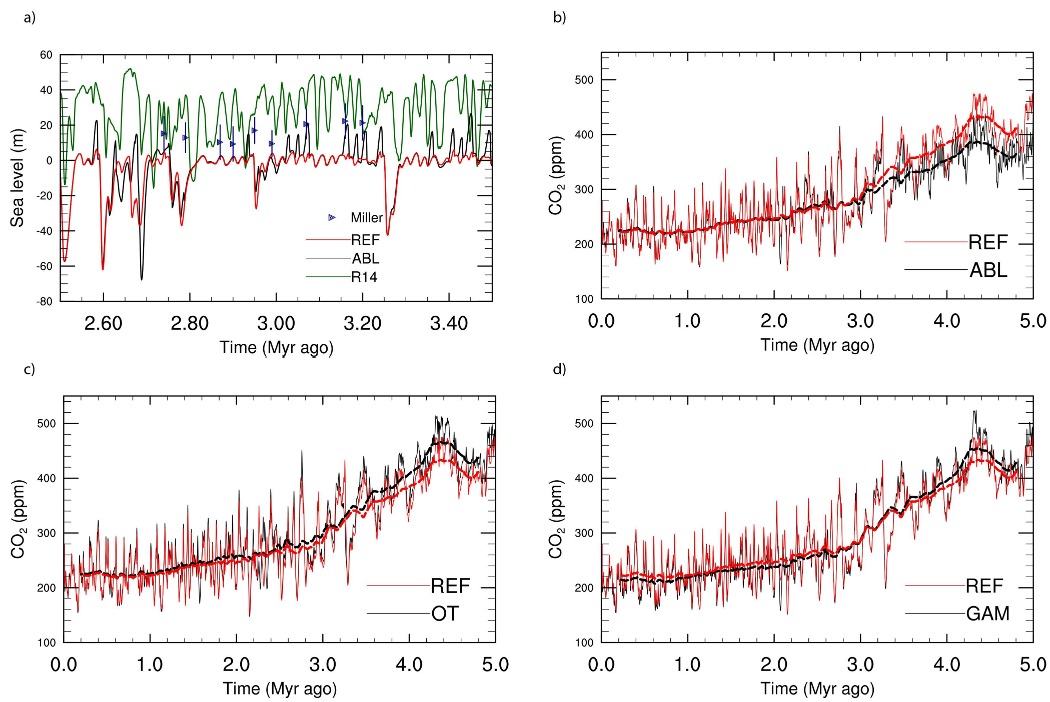

Figure 6: Simulated sea level and CO_2 concentrations. ***(a)*** *Modeled sea level over the Late Pliocene period 3.5 to 2.5 Myr ago and* ***(b-d)*** *modeled* CO_2 *over the past five million years. In red, our reference simulation; in black, simulations with increased Antarctic ablation (ABL), fixed pre-industrial ocean overturning strength (OT), and a smaller influence of deep-sea temperature on benthic* δ^{18}O *(GAM). The green line in panel* ***(a)*** *shows the sea level reconstruction of Rohling et al. (2014)[R14], interpolated to 100-year resolution. The blue triangles (Miller) in panel* ***(a)*** *represent a multi-method proxy data reconstruction of peak sea level (Miller et al., 2012), with error bars as indicated by that study. The thick dashed lines in panel* ***(b-d)*** *represent 400-kyr running averages.*

3.2.1. Influence of stability East Antarctica

In our reference experiment, we simulate a very stable Pliocene Antarctic ice sheet, leading to small variability in sea level. This is in agreement with earlier modelling studies (Huybrechts, 1993; Pollard and DeConto, 2009; De Boer et al., 2014) as well as some data studies (Denton et al., 1993). However, there are also other data suggesting that sea level was more variable during this time (Masson-Delmotte et al., 2013; Miller et al., 2012; Rohling et al., 2014; Cook et al., 2013). In a sensitivity experiment (ABL), we lower (in absolute sense) the ablation threshold parameter C_{abl} (Eq. 2) for the East Antarctic ice sheet from -30 to -5 during the entire run. This altered value leads to ablation starting at lower temperatures and hence to a decreased glaciation threshold in our model. The initial tuning target of Antarctic glaciation starting at around 750 ppm CO_2 (Stap et al., 2014) is thus compromised. However, this glaciation threshold is debated and it is suggested to be model-dependent (Hansen et al., 2013; Gasson et al., 2014).

In the ABL run, there is still very little surface melt on East Antarctica during the past 2.7 Myr. Therefore, modeled sea level remains approximately the same as in our reference simulation. Conversely, during the Pliocene sea level now varies between 5 m below and 30 m above present; it reaches up to +20 m during the Late Pliocene (Fig. 6a, black line). This corresponds better to a recent multi-method proxy data reconstruction of peak sea-level height (Miller et al., 2012) than our reference-run sea level (Fig. 6a, red line). However, continuous high sea level, such as reconstructed by Rohling et al. (2014) (Fig. 6a, [R14], green line), cannot be reconciled with the δ^{18}O input by our model.

As a consequence of the increased amount of ice volume variability during this time leading to a strengthening of the albedo-temperature feedback, we expect to find lower Pliocene CO_2 levels. Indeed, Pliocene CO_2 levels are reduced with respect to our reference (Fig. 6b). The difference is at most 70 ppm, but the average decrease over the period 5 to 2.7 Myr ago is only 28.5 ppm. The effect is relatively limited because, in our model, the grassland vegetation that replaces the retreated ice remains snow-covered throughout most of the year. The surface albedo reduction, which is the dominant effect of land ice on climate (Stap et al., 2014), is therefore small on the Antarctic continent. Hence, even if sea level variability is increased during the Pliocene, CO_2 concentrations remain significantly higher than reconstructed by Van de Wal et al. (2011). Alternatively, if EAIS variations are driven by marine-based instabilities as suggested by Pollard et al. (2015), the effect may be different, as this would not leave ice-free land when the EAIS retreats but rather open or sea-ice-covered ocean. Our one-dimensional SIA-based ice sheet model cannot reproduce such effects.

3.2.2. Influence of ocean overturning strength

In our reference run, the strength of the meridional ocean overturning is determined by the difference in temperature between polar and equatorial waters (Stap et al., 2014). To test the influence of this formulation, we conduct a separate run of the model where we keep overturning fixed at pre-industrial strength (run OT). In a similar way, Stap et al. (2014) inferred only little influence of the overturning strength on simulated temperature and ice volume during the past 800 thousand years. During the Pleistocene and

Holocene (2.5 Myrs ago to PD), the effect of fixing the strength on modeled CO_2 is indeed also limited (Fig. 6c). The simulated CO_2 in OT is on average 4.3 ppm higher than in the reference run. During the Pliocene (5 to 2.5 Myrs ago), this difference increases to 19 ppm. In run OT, overturning strength no longer increases when the climate warms, as it does in the reference experiment. The consequent weaker downwelling leads to cooler deep-ocean temperatures. As compensation, higher CO_2 is simulated. The maximum difference between the long-term (400 kyr) running averages of both simulations is 33 ppm, and occurs during the early Pliocene. We conclude that the effect of increased ocean overturning strength on simulated CO_2 becomes important during climates significantly warmer than pre-industrial in our model. Moreover, the M2 δ^{18}O excursion 3.3 Myr ago is not fully captured in run OT (not shown), marking the importance of variable meridional ocean overturning during this event.

Although ocean circulation is allowed to change, our model is forced only by insolation and CO_2. Independent changes in ocean circulation, for instance resulting from tectonic movement, are not incorporated. Furthermore, we do not take into account any vegetation changes. However, Foster and Rohling (2013) found that these processes only play a secondary role in long-term climate change over our simulated period.

3.2.3. Influence of relation between deep-sea temperature and δ^{18}O

The parameter γ (Eq. 3), relating deep-sea-temperature to benthic δ^{18}O may be debated. Therefore, it is a factor of model uncertainty. In our reference run it is taken from a paleotemperature equation (Duplessy et al., 2002): $0.28‰\text{K}^{-1}$. However, Marchitto et al. (2014) suggested a lower value of 0.22‰ K^{-1}. We implement this lower value for γ in run GAM. In this run, larger changes in CO_2 with respect to PI have to compensate the decreased effect of deep-sea temperature on $\delta^{18}O$ (Fig. 6d). Indeed, the CO_2 we simulate during the Pliocene is generally higher than our reference experiment (on average 8.4 ppm), and lower during the Pleistocene and Holocene (7.4 ppm). The long-term averages differ maximally 23.4 ppm. The model uncertainty imposed by the precise calculation of benthic $\delta^{18}O$ is therefore modest.

3.3. Comparison with existing and new proxy data

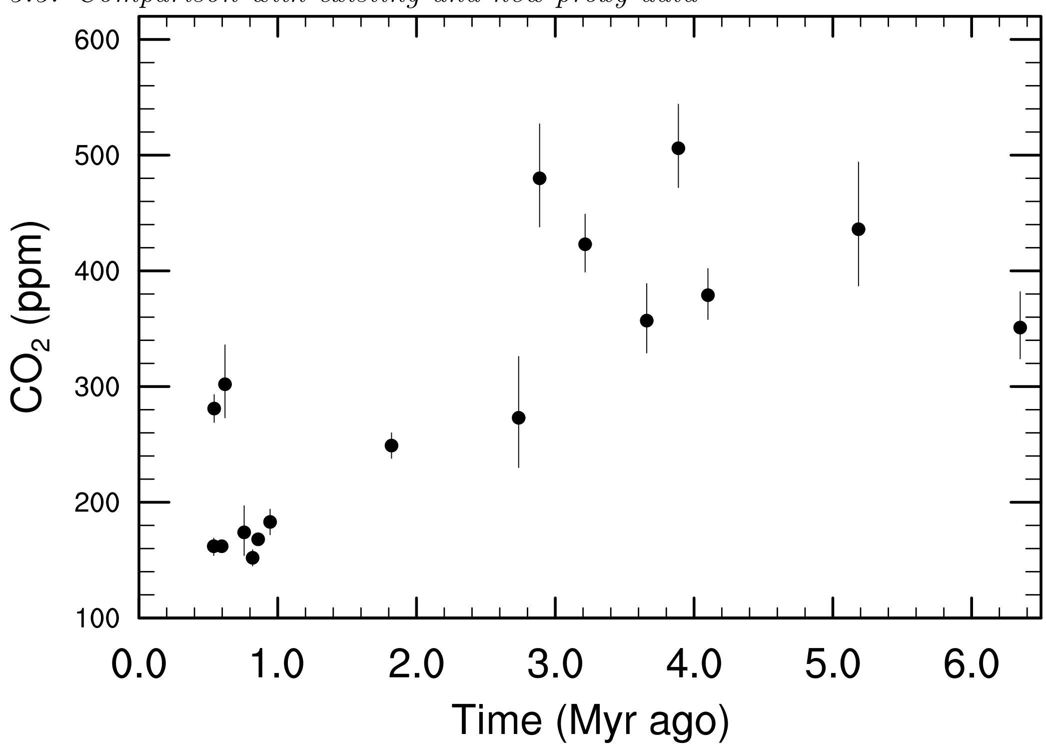

Figure 7: New CO_2 data. *New proxy-CO_2 data based on foraminiferal $\delta^{11}B$, derived from Integrated Ocean Drilling Program (IODP) Site 1264 on the Walvis Ridge in the South Atlantic subtropical gyre.*

New foraminiferal boron isotope based CO_2 data is derived from Integrated Ocean Drilling Program (IODP) Site 1264 on the Walvis Ridge in the South Atlantic subtropical gyre (Sect. 2.3). This data is shown is Fig. 7. We compare our model results to a compilation of CO_2 records obtained from alkenones (Fig. 8a), and from foraminiferal δ^{11}B including this new data (Fig. 8b).

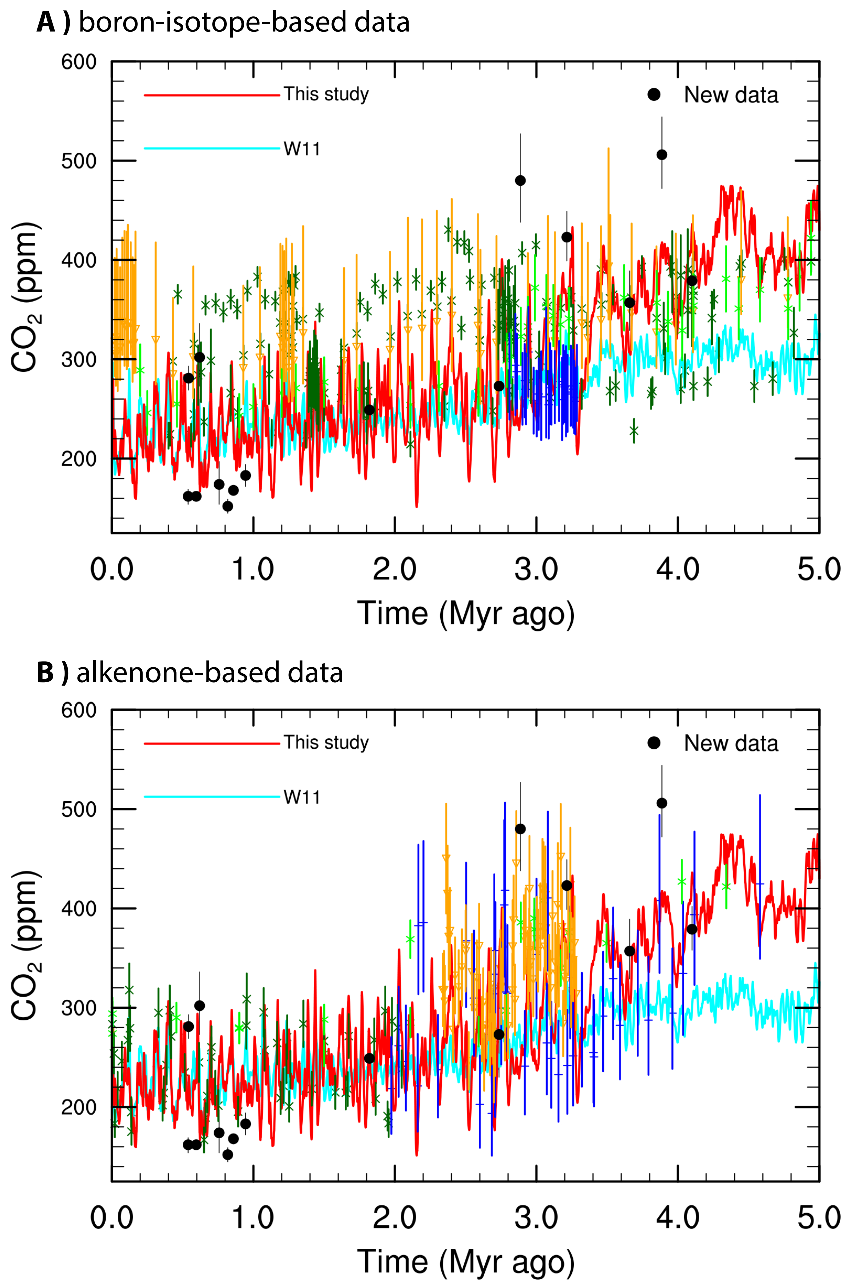

Figure 8: CO_2 **model-data comparison.** *The red line shows our simulated* CO_2 *record. The cyan line shows the hybrid model-data reconstruc-*

tion of Van de Wal et al. (2011) [W11]. The black dots indicate our new δ^{11}B-*based data, with error bars based on the standard deviation of repeated measurements.* ***(a)*** *Comparison with alkenone-based* CO_2 *data. Symbols indicate alkenone-based proxy* CO_2 *data (Zhang et al. (2013), orange triangles; Seki et al. (2010), lightgreen asterisks; Badger et al. (2013), blue plusses; Pagani et al. (2010), darkgreen crosses), with different error bars as indicated by these studies.* ***(b)*** *Comparison with boron-isotope-based* CO_2 *data. Symbols indicate previously published* δ^{11}B-*based proxy* CO_2 *data (Martínez-Botí et al. (2015a), orange triangles; Seki et al. (2010), lightgreen asterisks; Bartoli et al. (2011), blue plusses; Hönisch et al. (2009), darkgreen crosses), with different error bars as indicated by these studies.*

Over the past 2 million years, the model results, as well as the new data, are largely consistent with Hönisch et al. (2009) and Seki et al. (2010). Although the RMSE of our simulation with respect to Hönisch et al. (2009) (43.6 ppm) is larger than the RMSE of Van de Wal et al. (2011) (26.4 ppm), the increased variability in our simulation during this time, demonstrated by standard deviation (SD) of 33.8 ppm to 20.2 ppm in Van de Wal et al. (2011), agrees better with Hönisch et al. (2009) (SD=38.9 ppm). However, the simulation varies with a larger frequency than is reconstructed by the data. Therefore, model-data comparison would benefit from a more extensive data record. The high CO_2 levels in the alkenone-based records of Zhang et al. (2013) and Pagani et al. (2010) are not supported by our model.

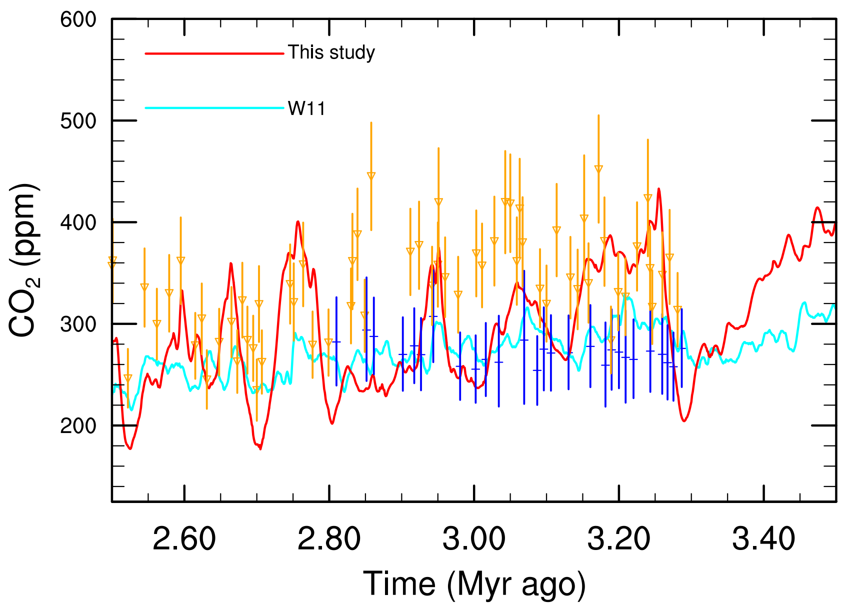

Figure 9: CO_2 **model-data comparison.** *Zoom-in on the Late Pliocene period 3.5 to 2.5 Myr ago, showing the data records with the highest resolution: Martínez-Botí et al. (2015a) (orange triangles), and Badger et al. (2013), blue plusses. The red line shows our simulated* CO_2 *record. The cyan line shows the hybrid model-data reconstruction of Van de Wal et al. (2011) [W11].*

In the Late Pliocene period (3.5 to 2.5 Myr ago), our modeled CO_2 variability agrees more with the record of Martínez-Botí et al. (2015a), than with the stable CO_2 concentrations shown by Badger et al. (2013) (Fig. 9). However, the RMSE (76.2 ppm) and model bias (-46.1 ppm) with respect to Martínez-Botí et al. (2015a) are quite high, albeit smaller than those of Van de Wal et al. (2011) (RMSE=87.1 ppm, bias=-73.1 ppm). The large simulated drop in CO_2 around 2.75 Myr ago is supported by the records of

Martínez-Botí et al. (2015a) and Bartoli et al. (2011). Conversely, we do not model high CO_2 values around 2.9 Myr ago, where the boron-isotope based records, as well as Pagani et al. (2010), agree upon. This most likely signifies a discrepancy between the benthic $\delta^{18}O$ record and the proxy CO_2 data.

Proxy CO_2 data are particularly scarce before 3.5 million years ago. Therefore, it is difficult to evaluate the reduced CO_2 variability in our simulation with respect to the Late Pliocene and Pleistocene. However, our higher CO_2 values than Van de Wal et al. (2011) seem to agree more favorably with the boron-isotope based records, including the new data, then with the alkenone-based record of Pagani et al. (2010).

4. Summary and conclusion

We have presented a continuous simulation of CO_2 over the past five million years. It is obtained using a coupled ice-sheet climate model, forced inversely by a stacked benthic $\delta^{18}O$ record (Lisiecki and Raymo, 2005). Therefore, the simulated CO_2 is in mutual agreement with modeled benthic $\delta^{18}O$, global sea level and temperature. As such, the records capture our understanding of the interaction between CO_2, sea level and the climate.

Our results clearly show that the relation between CO_2 and global temperature that holds over the ice-core period cannot be extended into the Pliocene. During this time, a weakening of the albedo-temperature feedback with the absence of large Northern Hemisphere ice sheets reduces Earth System Sensitivity (ESS). Our resuls show more variable and generally higher CO_2 values during the Pliocene than an earlier study that hypothesised constant ESS (Van de Wal et al., 2011).

The model results are modestly affected by the ocean overturning strength, as well as by the amplitude of the deep-sea temperature effect on benthic $\delta^{18}O$. Compared to the reference run, decreased strength of the overturning, as well as a weaker influence of deep-sea temperature, lead to smaller changes in benthic $\delta^{18}O$ at the same CO_2 concentrations. Hence, the simulated changes in CO_2 are larger.

In our reference simulation, the East Antarctic ice sheet (EAIS) is very stable during the Pliocene. When the ablation on the EAIS is increased, it is more dynamic, and consequently the Pliocene sea level is more variable. Peak sea level is then in better agreement with the multi-proxy synthesis of Miller et al. (2012). The increased sea level variability affects the simulated CO_2, but only to a relatively minor extent. This is explained by the ice-free land remaining snow-covered throughout most of the year, resulting in relatively small changes of the surface albedo.

Our simulated CO_2 is in broad agreement with existing and new $\delta^{11}B$-based proxy-CO_2 data. Although RMSE and model bias remain large, these records are generally more in line with the modeled variability during the Late Pliocene and Early Pleistocene than alkenone-based CO_2 records. They also agree more with the higher CO_2 simulated during the Early Pliocene. This means that the CO_2 concentrations obtained from the $\delta^{11}B$ proxy are more easily reconcilable with the benthic $\delta^{18}O$ record.

For higher-than-PI levels of CO_2, the reconstruction of Van de Wal et al. (2011) is predominantly determined by seemingly low CO_2 values (400-500 ppm) documented by proxy data during the Middle Miocene. We attain these values already during the Pliocene, when benthic $\delta^{18}O$ is higher. Benthic $\delta^{18}O$ is approximately equally low during the Middle Miocene as during the Late Eocene, when much larger CO_2 concentrations are reconstructed by the same proxies. In future research, we will extent our simulation further back in time and investigate this apparent conundrum.

Supplementary Data Figures

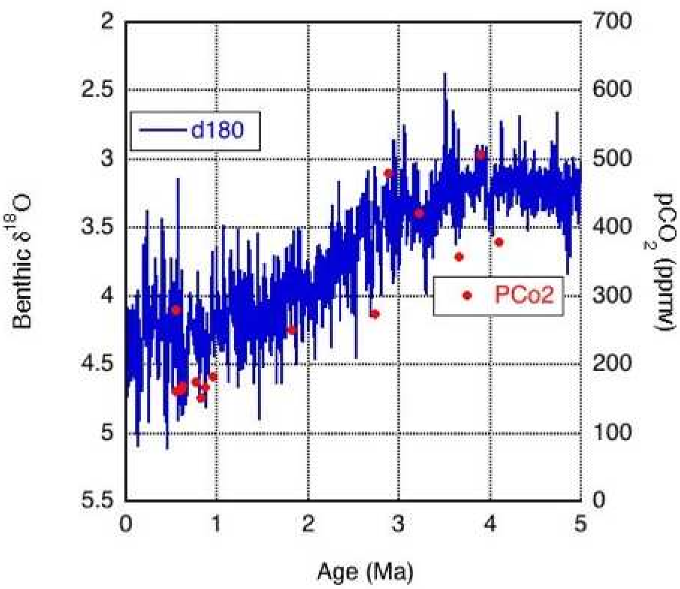

Supplementary Data Figure 1. *Planktic foraminiferal boron isotope based* pCO_2 *reconstructions from IODP Site 1264 (red dots) and the benthic foraminiferal oxygen isotope record of Site 1264 (grey line, Bell et al. (2014)).*

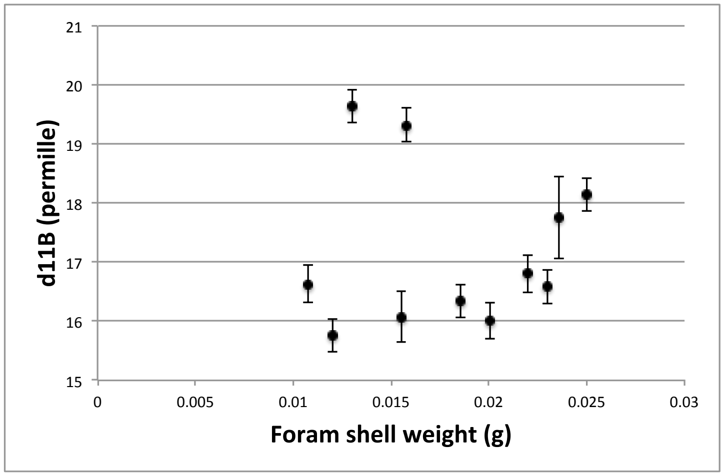

Supplementary Data Figure 2. *Planktic foraminiferal* δ^{11}B *with analytical error bars versus foraminiferal shell weight measured after cleaning. No correlation between shell weight and* δ^{11}B *values suggests that the picked foraminifer shells used for* δ^{11}B *analysis are unlikely to be biased by dissolution.*

Acknowledgements

Financial support was provided by the Netherlands Organisation of Scientific Research (NWO). M.Z. was financially supported by NWO Rubicon grant 019.2009.2.310.057. B.d.B. was financially supported by the Netherlands Earth System Science Centre (NWO). We thank Kenneth G. Miller for sharing his sea level data and Bärbel Hönisch for making the TIMS facility at LDEO for Boron Isotope measurements available and for the support during the analysis. We would further like to thank Markus Raitzsch, Orit Hyams and Nina Ruprecht for technical and analytical support of the boron data analysis. The Ocean Drilling Program (ODP) is thanked for supplying samples. Finally, we would like to thank three anonymous referees and the editor for providing useful suggestions, which helped to improve the quality of the paper.

References

Annan, J., Hargreaves, J., 2013. A new global reconstruction of temperature changes at the Last Glacial Maximum. Climate of the Past 9 (1), 367–376.

Austermann, J., Mitrovica, J. X., Latychev, K., Milne, G. A., 2013. Barbados-based estimate of ice volume at Last Glacial Maximum affected by subducted plate. Nature Geoscience 6 (7), 553–557.

Badger, M. P., Schmidt, D. N., Mackensen, A., Pancost, R. D., 2013. High-resolution alkenone palaeobarometry indicates relatively stable pCO_2 during the Pliocene (3.3-2.8 ma). Philosophical Transactions of the Royal Society of London A: Mathematical, Physical and Engineering Sciences 371 (2001), 20130094.

Barker, S., Greaves, M., Elderfield, H., 2003. A study of cleaning procedures used for foraminiferal Mg/Ca paleothermometry. Geochemistry, Geophysics, Geosystems 4 (9).

Bartoli, G., Hönisch, B., Zeebe, R. E., 2011. Atmospheric CO_2 decline during the Pliocene intensification of Northern Hemisphere glaciations. Paleoceanography 26 (4).

Beerling, D. J., Royer, D. L., 2011. Convergent Cenozoic CO_2 history. Nature Geoscience 4 (7), 418–420.

Bell, D., Jung, S., Kroon, D., Lourens, L., Hodell, D., 2014. Local and regional trends in Plio-Pleistocene δ^{11}B records from benthic foraminifera. Geochem. Geophys. Geosyst. 15, 3304–3321.

Bintanja, R., 1997. Sensitivity experiments performed with an energy balance atmosphere model coupled to an advection-diffusion ocean model. Theoretical and Applied Climatology 56 (1-2), 1–24.

Bintanja, R., Van de Wal, R.S.W., 2008. North American ice-sheet dynamics and the onset of 100,000-year glacial cycles. Nature 454 (7206), 869–872.

Cook, C. P., van de Flierdt, T., Williams, T., Hemming, S. R., Iwai, M., Kobayashi, M., Jimenez-Espejo, F. J., Escutia, C., González, J. J., Khim, B.-K., et al., 2013. Dynamic behaviour of the East Antarctic ice sheet during Pliocene warmth. Nature Geoscience 6 (9), 765–769.

Cuffey, K., 2000. Methodology for use of isotopic climate forcings in ice sheet models. Geophysical Research Letters 27 (19), 3065–3068.

De Boer, B., Lourens, L. J., van de Wal, R. S. W., 2014. Persistent 400,000-year variability of Antarctic ice volume and the carbon cycle is revealed throughout the Plio-Pleistocene. Nature Communications 5, doi:10.1038/ncomms3999.

De Boer, B., Van de Wal, R.S.W., Bintanja, R., Lourens, L.J., Tuenter, E., 2010. Cenozoic global ice-volume and temperature simulations with 1-

d ice-sheet models forced by benthic δ^{18}O records. Annals of Glaciology 51 (55), 23–33.

Dekens, P., Kynett, K., Wojcieszek, D., 2012. Plio-Pleistocene records from the south east Atlantic reveal changes in the Agulhas leakage. In: AGU Fall Meeting Abstracts. Vol. 1. p. 2040.

Denton, G. H., Sugden, D. E., Marchant, D. R., Hall, B. L., Wilch, T. I., 1993. East Antarctic ice sheet sensitivity to Pliocene climatic change from a dry valleys perspective. Geografiska Annaler. Series A. Physical Geography, 155–204.

Duplessy, J.-C., Labeyrie, L., Waelbroeck, C., 2002. Constraints on the ocean oxygen isotopic enrichment between the Last Glacial Maximum and the Holocene: Paleoceanographic implications. Quaternary Science Reviews 21 (1), 315–330.

EPICA community members, 2004. Eight glacial cycles from an Antarctic ice core. Nature 429 (6992), 623–628.

Foster, G., Pogge von Strandmann, P., Rae, J., 2010. Boron and magnesium isotopic composition of seawater. Geochemistry, Geophysics, Geosystems 11 (8).

Foster, G. L., Hönisch, B., Paris, G., Dwyer, G. S., Rae, J. W., Elliott, T., Gaillardet, J., Hemming, N. G., Louvat, P., Vengosh, A., 2013. Interlaboratory comparison of boron isotope analyses of boric acid, seawater and marine CaCO 3 by MC-ICPMS and NTIMS. Chemical Geology 358, 1–14.

Foster, G. L., Rohling, E. J., 2013. Relationship between sea level and climate forcing by CO_2 on geological timescales. Proceedings of the National Academy of Sciences 110 (4), 1209–1214.

Gasson, E., Lunt, D., DeConto, R., Goldner, A., Heinemann, M., Huber, M., LeGrande, A., Pollard, D., Sagoo, N., Siddall, M., et al., 2014. Uncertainties in the modelled CO_2 threshold for Antarctic glaciation. Climate of the Past 10 (2), 451–466.

Gasson, E., Siddall, M., Lunt, D. J., Rackham, O. J., Lear, C. H., Pollard, D., 2012. Exploring uncertainties in the relationship between temperature, ice volume, and sea level over the past 50 million years. Reviews of Geophysics 50 (1).

Grant, K., Rohling, E., Ramsey, C. B., Cheng, H., Edwards, R., Florindo, F., Heslop, D., Marra, F., Roberts, A., Tamisiea, M., et al., 2014. Sea-level variability over five glacial cycles. Nature Communications 5.

Hansen, J., Sato, M., Russell, G., Kharecha, P., 2013. Climate sensitivity, sea level and atmospheric carbon dioxide. Phil Trans R Soc A 3137, 20120294, doi:10.1098/rsta.2012.0294.

Haywood, A., Hill, D., Dolan, A., Otto-Bliesner, B., Bragg, F., Chan, W.-L., Chandler, M., Contoux, C., Dowsett, H., Jost, A., et al., 2013. Large-scale features of Pliocene climate: results from the Pliocene model intercomparison project. Climate of the Past 9, 191–209.

Hönisch, B., Hemming, N. G., 2004. Ground-truthing the boron isotope-paleo-pH proxy in planktonic foraminifera shells: Partial dissolution and shell size effects. Paleoceanography 19 (4).

Hönisch, B., Hemming, N. G., Archer, D., Siddall, M., McManus, J. F., 2009. Atmospheric carbon dioxide concentration across the Mid-Pleistocene Transition. Science 324 (5934), 1551–1554.

Huybrechts, P., 1993. Glaciological modelling of the late Cenozoic East Antarctic ice sheet: Stability or dynamism? Geografiska Annaler. Series A. Physical Geography, 221–238.

Klochko, K., Kaufman, A. J., Yao, W., Byrne, R. H., Tossell, J. A., 2006. Experimental measurement of boron isotope fractionation in seawater. Earth and Planetary Science Letters 248 (1), 276–285.

Laskar, J., Robutel, P., Joutel, F., Gastineau, M., Correia, A., Levrard, B., et al., 2004. A long-term numerical solution for the insolation quantities of the Earth. Astronomy & Astrophysics 428 (1), 261–285.

Lhomme, N., Clarke, G. K., Ritz, C., 2005. Global budget of water isotopes inferred from polar ice sheets. Geophysical Research Letters 32 (20).

Lisiecki, L. E., Raymo, M. E., 2005. A Pliocene-Pleistocene stack of 57 globally distributed benthic δ^{18}O records. Paleoceanography 20 (1).

Lunt, D. J., Haywood, A. M., Schmidt, G. A., Salzmann, U., Valdes, P. J., Dowsett, H. J., 2010. Earth System Sensitivity inferred from Pliocene modelling and data. Nature Geoscience 3 (1), 60–64.

Marchitto, T., Curry, W., Lynch-Stieglitz, J., Bryan, S., Cobb, K., Lund, D., 2014. Improved oxygen isotope temperature calibrations for cosmopolitan benthic foraminifera. Geochimica et Cosmochimica Acta 130, 1–11.

Martínez-Botí, M., Foster, G., Chalk, T., Rohling, E., Sexton, P., Lunt, D., Pancost, R., Badger, M., Schmidt, D., 2015a. Plio-Pleistocene climate sensitivity evaluated using high-resolution CO_2 records. Nature 518 (7537), 49–54.

Martínez-Botí, M., Marino, G., Foster, G., Ziveri, P., Henehan, M., Rae, J., Mortyn, P., Vance, D., 2015b. Boron isotope evidence for oceanic carbon dioxide leakage during the last deglaciation. Nature 518 (7538), 219–222.

Masson-Delmotte, V., Schulz, M., Abe-Ouchi, A., Beer, J., Ganopolski, A., GonzalezRouco, J., Jansen, E., Lambeck, K., Luterbacher, J., Naish, T., Osborn, T., Otto-Bliesner, B., Quinn, T., Ramesh, R., Rojas, M., Shao, X., Timmermann, A., 2013. Information from Paleoclimate Archives. Cambridge University Press, Cambridge, United Kingdom and New York, NY, USA, book section 5, p. 383464.

Miller, K. G., Wright, J. D., Browning, J. V., Kulpecz, A., Kominz, M., Naish, T. R., Cramer, B. S., Rosenthal, Y., Peltier, W. R., Sosdian, S., 2012. High tide of the warm Pliocene: Implications of global sea level for Antarctic deglaciation. Geology 40 (5), 407–410.

North, G. R., 1975. Theory of energy-balance climate models. Journal of the Atmospheric Sciences 32 (11), 2033–2043.

Pagani, M., Liu, Z., LaRiviere, J., Ravelo, A. C., 2010. High Earth-system climate sensitivity determined from Pliocene carbon dioxide concentrations. Nature Geoscience 3 (1), 27–30.

Pollard, D., DeConto, R. M., 2009. Modelling West Antarctic ice sheet growth and collapse through the past five million years. Nature 458 (7236), 329–332.

Pollard, D., DeConto, R. M., Alley, R. B., 2015. Potential Antarctic ice sheet retreat driven by hydrofracturing and ice cliff failure. Earth and Planetary Science Letters 412, 112–121.

Rohling, E., Foster, G., Grant, K., Marino, G., Roberts, A., Tamisiea, M., Williams, F., 2014. Sea-level and deep-sea-temperature variability over the past 5.3 million years. Nature 508 (7497), 477–482.

Seki, O., Foster, G. L., Schmidt, D. N., Mackensen, A., Kawamura, K., Pancost, R. D., 2010. Alkenone and boron-based Pliocene pCO_2 records. Earth and Planetary Science Letters 292 (1), 201–211.

Shipboard Scientific Party, 2004. Leg 208 Summary. Ocean Drilling Program, College Station, TX, USA, pp. 1–112.

Stap, L.B., van de Wal, R.S.W., de Boer, B., Bintanja, R., Lourens, L.J., 2014. Interaction of ice sheets and climate during the past 800 000 years. Climate of the Past 10 (6), 2135–2152.

Tyrrell, T., Zeebe, R. E., 2004. History of carbonate ion concentration over the last 100 million years. Geochimica et Cosmochimica Acta 68 (17), 3521–3530.

Van de Wal, R. S. W., de Boer, B., Lourens, L. J., Köhler, P., Bintanja, R., 2011. Reconstruction of a continuous high-resolution CO_2 record over the past 20 million years. Climate of the Past 7 (4), 1459–1469.

Zachos, J. C., Dickens, G. R., Zeebe, R. E., 2008. An early Cenozoic perspective on greenhouse warming and carbon-cycle dynamics. Nature 451 (7176), 279–283.

Zhang, Y. G., Pagani, M., Liu, Z., Bohaty, S. M., DeConto, R., 2013. A 40-million-year history of atmospheric CO_2. Philosophical Transactions of the Royal Society of London A: Mathematical, Physical and Engineering Sciences 371 (2001), 20130096.